Published in final edited form as:
Hörth, R. M., Kerschnitzki, M., Aido, M., Schmidt, I., Burghammer, M., Duda, G. N., et al. (2017). Correlations between nanostructure and micromechanical properties of healing bone. *Journal of the Mechanical Behavior of Biomedical Materials*. doi:10.1016/j.jmbbm.2017.08.022.

Correlations between nanostructure and micromechanical properties of healing bone

Rebecca M. Hörth, Michael Kerschnitzki, Marta Aido, Ingo Schmidt, Manfred Burghammer, Georg N. Duda, Peter Fratzl, Bettina M. Willie, Wolfgang Wagermaier

Graphical Abstract

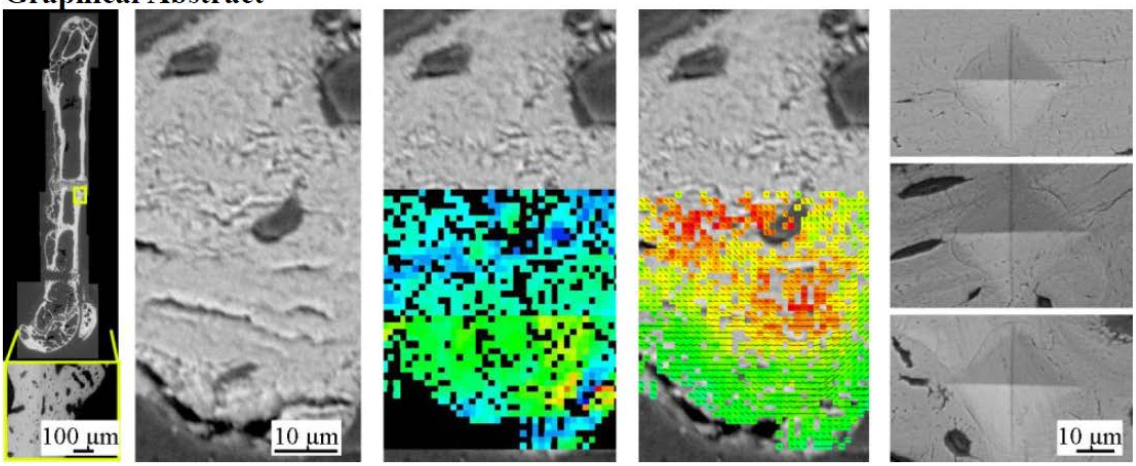

Highlights

- In callus tissue, woven bone islands are surrounded by lamellar bone.
- Degree of mineralization in callus tissue correlates with mineral particle size.
- Cortical, callus lamellar and callus woven bone areas show different hardness.
- Different bone types lead to varying crack propagation patterns.

Correlations between nanostructure and micromechanical properties of healing bone

Rebecca M. Hörth[a,b], Michael Kerschnitzki[a], Marta Aido[b,c], Ingo Schmidt[a], Manfred Burghammer[d], Georg N. Duda[c], Peter Fratzl[a], Bettina M. Willie[c,e], Wolfgang Wagermaier[a,*]

[a] Max Planck Institute of Colloids and Interfaces, Department of Biomaterials, Research Campus Golm, 14424 Potsdam, Germany

[b] Berlin-Brandenburg School for Regenerative Therapies (BSRT), Charité - Universitätsmedizin Berlin, Augustenburger Platz 1, 13353 Berlin, Germany

[c] Julius Wolff Institute & Center for Musculoskeletal Surgery, Charité - Universitätsmedizin Berlin, Augustenburger Platz 1, Institutsgebäude Süd, 13353 Berlin, Germany

[d] European Synchrotron Radiation Facility, BP220, 38043 Grenoble Cedex 9, France

[e] Research Centre, Shriners Hospitals for Children-Canada, Department of Pediatric Surgery, McGill University, 1003 Decarie Blvd, Montreal, Quebec, Canada, H4A 0A9

[*]Corresponding Author:

Dr. Wolfgang Wagermaier

Max Planck Institute of Colloids and Interfaces

Department of Biomaterials

Research Campus Golm

14424 Potsdam, Germany

Phone: +49 (0) 331 567 9459

wolfgang.wagermaier@mpikg.mpg.de

Abstract

All hierarchical levels in bone are known to contribute to its mechanical behavior. The basic building block is the mineralized collagen fibril which is assembled into larger structures with varying fibrillar organization. The collagen organization increases from unordered woven bone in the callus which is gradually replaced by higher ordered lamellar bone during bone development and healing and finally results in cortical lamellar bone with highest degree of organization. The structural and mechanical description of these organizational motifs is not yet complete.

We investigated a femoral osteotomy mouse model and analyzed newly formed callus tissue and mature lamellar bone in the cortex. This model exhibits three bone types with different fibrillar organization: (i) woven, (ii) moderate lamellar and (iii) lamellar. Using high resolution synchrotron small angle X-ray scattering in combination with back-scattered electron imaging we characterized the ultrastructure of the different regions in terms of degree of mineralization, averaged mineral particle thickness and mineral particle orientation. We further used microindentation to correlate hardness, induced crack lengths and crack patterns with the bone ultrastructure.

The newly formed callus tissue contains highly mineralized woven bone islands, featuring thick but poorly ordered mineral particles. Such islands are surrounded by layers of lamellar bone with a low mineralization level and thin but well aligned particles. Callus tissue shows lower hardness values and longer cracks than the cortex. Callus woven bone exhibits shorter cracks than callus lamellar bone. However, the poorly mineralized callus lamellar bone shows crack propagation mechanisms similar to cortical bone due to its very similar lamellar organization and high degree of mineral particle orientation.

In conclusion we demonstrate that woven and increasingly higher oriented lamellar bone do not only differ in collagen fibril organization, but also that the amount, orientation and different shape of mineral particles are also likely to contribute to the reduced mechanical

competence of woven as compared to lamellar bone. This may explain why many organisms replace less organized bone types with higher organized ones.

Highlights

- In callus tissue, woven bone islands are surrounded by lamellar bone.
- Degree of mineralization in callus tissue correlates with mineral particle size.
- Cortical, callus lamellar and callus woven bone areas show different hardness.
- Different bone types lead to varying crack propagation patterns.

1 Introduction

Nature forms bones with different structure and mechanical properties at the micro- and macroscale by varying the arrangement of the very same building blocks at the nanometer scale (Weiner and Wagner 1998, Currey 2002, Currey 2003). The most universal building block in bone is the mineralized collagen fibril, a composite made from collagen molecules and nanometer-sized hydroxyapatite mineral particles (Fratzl and Weinkamer 2007). The mineralized collagen fibrils are assembled to larger structures with different degrees of collagen organization (Reznikov, Shahar et al. 2014). During bone growth, two different types of bone are produced: (i) woven bone is formed rapidly and exhibits a relatively unordered collagen structure; (ii) later highly ordered lamellar bone forms on a pre-existing scaffold that can be made of either woven bone or a synthetic implant material (Currey 2002, Ferretti, Palumbo et al. 2002, Shapiro 2008, Kerschnitzki, Wagermaier et al. 2011, Cipitria, Lange et al. 2012) or replaces woven bone. This lamellar arrangement of fibers is made possible by a coordinated action of many bone forming cells starting from preexisting surfaces (Kerschnitzki, Wagermaier et al. 2011).

Bone types can be distinguished based on their collagen fibril organization, structure, composition and their resulting mechanical properties (Currey 2002). The long axis of the hydroxyapatite platelets is usually aligned with the collagen fibril orientation (Fratzl, Gupta et al. 2004). Woven bone usually includes numerous osteocytes, which have a roundish shape and are randomly distributed in the volume (Hernandez, Majeska et al. 2004, Hirose, Li et al. 2007, Kerschnitzki, Wagermaier et al. 2011). On the nanometer level, woven bone shows a poorly arranged collagen matrix and mineral particles with a low degree of alignment (Weiner and Wagner 1998). Woven bone is typically more highly mineralized (Currey 2002, Kerschnitzki, Wagermaier et al. 2011) than lamellar bone, and features relatively low

numbers of elongated osteocytes (Hernandez, Majeska et al. 2004, Hirose, Li et al. 2007, Kerschnitzki, Wagermaier et al. 2011). Mineral particles in lamellar bone show a high degree of alignment (Kerschnitzki 2012). Due to the higher degree of collagen matrix organization, lamellar bone material is believed to possess superior mechanical competences compared to woven bone material (Currey 2002).

Bone has a great potential to regenerate from damage and to adapt to changing environmental conditions (McKibbin 1978). There is evidence that bone regeneration processes are similar to bone formation processes during embryonic and fetal development, showing a similar appearance of different bone types over time. Callus formation includes two waves of bone formation, whereby a highly disordered woven bone is formed first, followed by lamellar bone deposition at the surface of the initially formed bone material (Liu, Manjubala et al. 2010, Kerschnitzki, Wagermaier et al. 2011, Hoerth, Seidt et al. 2014). Degree of collagen fibril alignment and mineral particle size within the callus continuously increases with healing time which also has an impact on the mechanical competence of such callus material (Manjubala, Liu et al. 2009, Liu, Manjubala et al. 2010, Hoerth, Seidt et al. 2014). A detailed investigation of correlations between nanoscopic bone structure and superior mechanical properties in bone tissue with different degrees of fibril organization remains challenging, mainly for two reasons: (i) the availability of bone with varying fibrillar organization from one individual is rare and (ii) structural and mechanical investigations from the same bone volume are experimentally difficult to achieve. Callus tissue is an ideal model system for these investigations because it contains different bone types with varying organization at the fibrillar level within one sample: woven bone, moderately organized lamellar bone in the callus and highly organized lamellar bone in the cortex.

The mechanical properties of bone can be described using various parameters (e.g. strength, stiffness and toughness), all indicating different aspects of mechanical behavior (Cowin 2001). Toughness of a material describes the ability to absorb energy during deformation before fracture occurs, strength is the capacity to withstand a certain force without fracturing, and stiffness relates to the force to deform a material. Bone material is known to be both stiff and tough (Fratzl, Gupta et al. 2004, Launey, Buehler et al. 2010). Toughness of bone depends in a complex way on the internal architecture of the material on all scales from nanometers to millimeters (Wagermaier, Klaushofer, Fratzl 2015). At the nanometer scale it is related to the plasticity of the fibril-mineral- and fibril-fibril-interfaces, while on higher scales it also depends on crack formation and propagation, because this absorbs energy. Compared to cracks in woven bone, the ones in lamellar bone are more easily deflected and have longer distances to run and therefore this bone type shows higher toughness preventing fracture (Koester, Ager et al. 2008).

The different mechanical properties of bone can be measured by different methods: Nanoindentation tests are used to determine the material's hardness by measuring the resistance against plastic deformation (Rho, Tsui et al. 1997, Zysset, Guo et al. 1999). On a larger scale, microindentation can also be used to measure hardness and in addition to provoke crack formation and to evaluate the resulting crack pattern and crack length to deduce mechanical properties (Kruzic, Kim et al. 2009), e.g. toughness. It is unclear if and how hardness can be directly related to toughness. According to the definition of Peterlik et al. (Peterlik, Roschger et al. 2006) toughness correlates to the energy dissipation during crack propagation within a material. Mechanisms like crack bridging due to collagen fibers across lamellae and crack deflection due to differently oriented collagen fibrils within subsequent lamellae dissipate energy Thus, crack length measurements can give estimates on the material's toughness.

The goal of this study is to measure mechanical properties of different bone types with varying fibrillar organization and to relate those to the bone nanostructure. We chose a mouse femoral osteotomy model, in which different bone types occur during healing: woven and lamellar bone in the callus as well as lamellar bone in the cortex. The mice included in our study showed comparable healing outcomes to previous bone healing studies in mice using the same fixation system (Kruck, Duda, et al. 2013 and Röntgen, Blakytny, et al. 2010). Although there is always some variation in healing outcome between animals, the external fixator facilitates a more standardized healing outcome compared to other fixation systems, such as intramedullary nails. We investigated: (i) the microstructural organization by back-scattered electron microscopy imaging, which allows classification of the bone types as lamellar cortical, woven callus and lamellar callus bone; (ii) the nanostructural organization, in particular the mineral particle thickness and orientation in relation to the corresponding bone type by small-angle X-ray scanning. Furthermore we measured (iii) the hardness of the specific bone types and deduced the toughness of the bone material by measuring the crack length.

2 Materials and Methods

2.1 Animal Model

The study included three animals (26 weeks old, female C57Bl/6J mice, weighting 22-25 g), group-housed in a cage, with ad libitum access to food and water. In each animal, a femoral osteotomy was performed on only the left limb, while the right limb served as an internal control. All mice were sacrificed on day 21 post-osteotomy, while under anesthesia, through an overdose of potassium chloride. All animal experiments described were carried out according to the policies and procedures approved by the local legal research animal welfare representative (LaGeSo Berlin, G0021/11).

2.2 Surgical Procedure and Sample Preparation

2.2.1 Surgery

For surgical preparation, the mice were weighed and then placed in a plexiglass box containing a 2% isoflurane-oxygen mixture. After achieving a sufficient depth of anesthesia, the anesthetic was given via a breathing mask maintaining a dose of 1.5-2% pure isoflurane oxygen mixture. To protect the eyes from drying, they are wetted with the eye ointment Bepanthen®. The mice were administered a single subcutaneous injection of the painkiller buprenorphine (Temgesic®, 0.1 mg / kg). To avoid infection, the mice were given a single subcutaneous injection of the antibiotic clindamycin (45 mg / kg). The left thigh was disinfected and shaved. The adequate anesthetic depth was ensured by checking the interdigital reflex. A small skin incision was performed between the hip and knee. The fascia lata, which is located between the Mm. gluteus superficialis and biceps femoris was bluntly dissected to the femur. The external fixator was mounted in cranio-lateral direction by inserting four mini-schanz screws (pins) (0.45 mm, RISystem, Switzerland) into the femur. The pins were connected to one another via a unilateral bar. After mounting the fixator, a 0.5 mm osteotomy gap was created using a gigli saw (0.44 mm, RISystem, Switzerland). The wound was closed with a suture of the muscle fascia and a suture of the skin. For pain management the animals received tramadol hydrochloride (25 mg/l) ad libitum in their drinking water, for three days following surgery. Plastic houses were removed from the cages to prevent injury, but extra paper was added to the cage for enrichment.

2.2.2 Sample Preparation

After dissection of both femora, the bones were directly transferred into 100% ethanol and stored at room temperature. Samples were then embedded in polymethyl methacrylate (PMMA) and cut into blocks of about 15*10*5 mm (each containing a single femur) using a low speed diamond saw (Buehler Isomet, Duesseldorf, Germany).

2.2.3 Measurement Regions

The callus regions contain structurally different bone types (organization of the fibrils) and therefore we defined three different regions across the entire bone: cortical bone (CB), newly formed lamellar bone in the callus (CL) in direct contact to pre-existing cortical bone and woven bone in the callus (CW). The BSE images were used to morphologically distinguish between the different structures referring to the degree of organization of the collagen fibrils: woven and lamellar bone within the callus and lamellar cortical bone.

2.3 Small Angle X-ray Scattering Experiments

2.3.1 Sample Preparation

Thin longitudinal sections of the embedded bones were produced using a microtome (Leica SM2500S, with a Leica VMH 400 knife, Nussloch, Germany). The sections were 6 µm thick and cutting was performed along the direction of the long axis of the bone approximately along the saggital planes of all samples. Saturated hydroxyapatite solution was used during cutting to prevent the mineral from dissolving during sectioning. Cutting was performed until the estimated center of the bone was reached. Sections were then put on 50 ± 5 µm thick silicon wafers (SI-MAT, Kaufering, Germany) and fixed on the wafers by air drying. The periosteal callus is the area at which bone formation starts. Thus to characterize the bone quality in callus formation, we selected this relevant and mature callus formation side. The remaining half block (thickness of about 5 mm) was used for microindentation tests.

2.3.2 Measurements

The small angle X-ray scattering (SAXS) experiments were performed at the Nanofocus beamline (ID 13) at the European Synchrotron Radiation Facility (ESRF, Grenoble, France). Regions of interest were defined, (i) pre-existing cortex and (ii) periosteal callus (at some distance from the osteotomy, where there is still remaining cortex in contact). For all

osteotomized samples, within the two regions of interest a smaller area was measured (861 measurement points for each cortex region and 6601-10836 measurement points within the callus region).

Briefly, the thin sections were fixed on silicon wafers and mounted on a sample holder, perpendicular to the beam path. The X-ray beam was focused to a size of 1 µm and the sample was then scanned by moving it in the x and y-direction with a motorized sample stage. The wavelength of the X-ray beam was 0.0984 nm (E=12.6 keV) and the measurement time was 0.8 s per point. The scattering patterns were recorded with a FReLon detector (2048 x 2048 pixels) with binning four, resulting in 512 x 512 pixels with a pixel size of 206.88 µm x 206.18 µm. The scattering patterns were corrected with a dark current and an empty beam measurement and were then integrated and further evaluated (next section).

2.3.3 Evaluation of the SAXS data

Evaluation of the SAXS data was performed with open source DPDAK software (directly programmable data analysis kit, https://dpdak.desy.de) (Benecke, Wagermaier et al. 2014). Corrected scattering patterns were integrated azimuthally and radially resulting in two dimensional intensity profiles. These were used to calculate various parameters, describing different characteristics of the mineral particles. As described in (Rinnerthaler, Roschger et al. 1999, Pabisch, Wagermaier et al. 2013), the *T* parameter values were derived from the scattering intensity I depending on the scattering vector q. The *T* parameter describes the ratio of volume to surface of the crystals (Fratzl, Fratzl-Zelman et al. 1991, Fratzl, Schreiber et al. 1996) and is defined as follows:

$$T = \frac{4\phi(1-\phi)}{\sigma}$$

ϕ is the total volume of mineral particles per unit volume and σ the total surface area per unit volume. Assuming plate-like shape for the mineral particles (Landis, Song et al. 1993, Landis,

Hodgens et al. 1996) and assuming the mineral volume fraction $\phi = 0.5$, then *T* represents the mean mineral particle thickness (Fratzl 1994).

The predominant direction of orientation and the ρ parameter, defined as the degree of orientation (values between 0 and 1) were calculated from the scattering intensity I depending on the angle χ (Rinnerthaler, Roschger et al. 1999, Pabisch, Wagermaier et al. 2013). A ρ parameter of 1 would correspond to perfectly aligned mineral particles within the exposed bone volume while a ρ parameter of 0 corresponds to a completely arbitrary distribution of particle orientation. The data was further processed using SigmaPlot 11 (Systat Software, San José, USA) and Origin 8G (OriginLab, Northampton, USA). Inadequately fitted data was excluded based on the criterions described in Pabisch, Wagermaier et al. 2013, mean values and standard deviations were calculated and color- and bar-coded maps were created to illustrate T parameter, direction of predominant orientation and ρ parameter. Finally the results were overlaid onto backscattered electron microscopy images (BSE), giving an impression of the surrounding bone structure, using Photoshop CS5 (Adobe Systems, Munich, Germany).

2.4 Microindentation

2.4.1 Sample preparation

The blocks of the embedded samples were ground and polished to create plano-parallel surfaces (PM5, Logitech, Glasgow, Scotland) and a surface roughness of about 0.02 µm. Care was taken that the surface was free of scratches and polishing damages to avoid topographical contrast artefacts in the backscattered electron imaging and in indentation depths.

2.4.2 Measurements

Indents were performed using a microhardness tester with a video measuring system and equipped with a Vickers indenter tip (MHT-10 from Anton Paar, Graz, Austria) attached to a light microscope (Leica DM RXA2, Wetzlar, Germany). A loading speed of 50 mN/s was used to obtain a maximum force of 500 mN. This force was held for a resting time of 30 s and then unloaded. The exact indentation positions were determined with a light microscope using an objective instead of the microindentation device and a magnification of 50x. Two samples from different individuals have been used for microindentation. The remaining block of the third individual was not suited for these experiments, since cutting the slices for SAXS did not leave enough material for indentation. In total we performed on a sample from one individual ten indents in cortical bone, eight indents in callus lamellar bone, and ten indents in callus woven bone (see Table 1). Hardness values represent mechanical information from the volume element where the indent has been made. Due to the anisotropic nature of bone the hardness values also depend on the orientation of the specific volume elements and therefore care has been taken that cutting along the bone axis was performed in a comparable way for all samples.

2.4.3 Evaluation

Vickers hardness has been calculated using the software of the microindentation device. Therefore the lengths of diagonals of the indent were measured using the light microscope (Leica DM RXA2, Wetzlar, Germany).

Crack patterns were then visualized with an electron microscope (BSE). The BSE images of the indents were compared with images of the pre-indented bone and then edited with ImageJ (http://imagej.nih.gov/ij/), see Supplementary Figure 1. Comparing the pre- and the post-indented image, the lengths of the newly formed cracks are measured (marked in yellow) using ImageJ and summed up to obtain the total crack length, resulting from the indent. The

total crack length is interpreted as a measure for toughness and has been used from different authors on hard tissue (Imbeni, Kruzic et al. 2005, Mullins, Bruzzi et al. 2007). This interpretation has been doubted recently (Kruzic, Kim et al. 2009), but our approach to apply several methods onto the same sample sections did not allow to perform additional indentations. This is also related to the limitation that the crack thickness is not implicated, and especially cortical indents show thin fissures that are also included (see white arrows).

2.5 Backscattered Electron Imaging

An environmental scanning electron microscope (ESEM, FEI Company, Oregon, USA) with a backscattered electron detector was used to qualitatively visualize the degree of mineralization (grey value) in the different bone sections. The PMMA blocks with the embedded bone have been polished but were not coated. Our settings were: acceleration voltage of 10 or 12.5 kV, low vacuum conditions (0.75 Torr), working distance of approximately 10 mm, and various magnifications (60 - 4000x). For the pre-characterization of samples measured with SAXS as well as for visualizing the results, a magnification of about 60x was used to provide overview images (e.g. Figure 2A). We used 200x or 250x for the regional overview images (Figure 2B) and 1000x to produce images of the local structure in more detail (Figure 3A and B). For evaluation of the microindentation experiments, images were taken at 2000x before and after indentation (Figure 1). BSE gives information about the mineralization of the tissue: grey values are related to calcium content as Ca is the element with the highest atomic number present within the tissue (Roschger, Gupta et al. 2003). Since bone matrix (collagen) is continuously mineralized during formation and remodeling, the grey values also indicate the tissue age (Fratzl, Gupta et al. 2004).

Table

Table 1: Vickers hardness and crack length of different bone types resulting from microindentation testing for one individual animal. Hardness (Vickers hardness) and crack length are given for every indentation point and as mean value and standard deviation for the different types of bone.

Hardness (HV)			Total crack length (µm)		
cortex (CB)	callus lamellar (CL)	callus woven (CW)	cortex (CB)	callus lamellar (CL)	callus woven (CW)
95.9	65.4	76.4	110.6	382.0	86.3
114.9	65.9	61.4	74.5	147.2	131.0
102.0	71.4	84.7	120.1	171.5	123.0
82.7	61.4	94.3	156.0	173.3	117.5
101.0	69.8	82.0	215.8	277.8	68.9
118.5	73.6	65.0	92.1	163.0	219.5
114.9	83.3	80.7	111.7	46.6	147.2
111.7	74.1	78.8	121.2	144.3	189.3
119.4		86.1	108.6		235.1
116.0		75.8	97.2		218.7
107.7 ± 11.9	70.6 ± 6.7	78.5 ± 9.7	120.8 ± 39.6	188.2 ± 100.3	153.6 ± 58.7

3 Results

3.1 Bone Type Identification by BSE

High resolution BSE images provide morphological and degree of mineralization information that allow for differentiation of the three bone types of interest:: (i) cortical bone (CB), (ii) callus woven bone (CW) and (iii) callus lamellar bone (CL).

CB (Figure 1, left column) remains from the pre-osteotomized stage and therefore is already identified based on its location. It typically has a relatively high degree of order at the micrometer (lamellar) scale representing a more homogenous material structure than woven bone at this length scale. It comprises only few, elongated osteocyte lacunae with their long axis parallel to the orientation of the bone lamellae (Figure 1 CB). The canaliculi, connecting the osteocyte lacunae appear to run perpendicular to the lamellar orientation and the osteocytes long axis (Kerschnitzki, Wagermaier et al. 2011). Figure 1 shows that cortical bone is also more homogeneously mineralized on the micrometer scale than the bone types in the callus, as revealed by the uniform BSE signal.

CW (Figure 1, central column), which is newly formed bone material deposited post-osteotomy. It is located within the callus tissue usually in the center of the newly formed callus bone struts. Such woven bone islands feature a low degree of fiber organization and encompass roundish shaped osteocyte lacunae. The degree of mineralization is higher as compared to the more organized surrounding tissue.

CL (Figure 1, right column) is characterized by a more lamellar appearance compared to CW, but compared to CB the lamellae appear only on a smaller length scale (few tens of microns). The osteocyte lacunae located within this tissue show an elongated shape parallel to the lamellar orientation. The degree of mineralization is low (darker grey values in BSE images), and lamellar bone often consists of only a small trabecula-like bone strut. These struts can be seen on a larger scale in the mineralizing callus in Figure 2 B. Thus both CB and newly

formed CL feature a lamellar structure, however, they show a different mineralization state due to their different tissue ages and are present at different anatomical locations (CB within the pre-existing cortex and CL within the newly formed callus).

3.2 Ultrastructure of different Bone Types revealed by X-ray scattering

Corresponding to the different microscopic structures as revealed by electron microscopy, the different bone types are expected to exhibit distinct nanostructural organization. High resolution SAXS was used to determine the degree of orientation (**ρ**) and the thickness of the mineral particles (**T**) and to indicate the presence and location of the different bone types.

CB shows a relatively high degree of mineral particle orientation (**ρ**) with the majority of scan regions featuring a mineral particle alignment of around 55 % of mineral particles being aligned along the main orientation axis parallel to the long axis of the bone (Figure 2 C and D, see Supplementary Figure 2 and 3 for three different animals). This confirms the lamellar organization of the cortex as revealed by back-scattered electron microscopy as the predominant structural motif. However, two of the scan regions show significantly less mineral particle alignment with a **ρ** parameter around 0.35. In the callus most of the scan regions show a very similar degree of mineral particle orientation around 0.35 indicating a rather disorganized bone structure and only a small fraction is present with high mineral particle orientation (> 0.4) similar to the highly organized lamellar regions in the cortex.

The average mineral particle thickness in CB regions is relatively high with average values around 3 nm as compared to the callus regions with average values around 2.6 nm. However the distribution of **T** is much broader in the callus which indicates not only a variety of tissue ages (different mineralization states) but also points towards the two different structural motifs of woven and lamellar bone present within the callus. The correlation between **ρ** and **T**

Figure 1

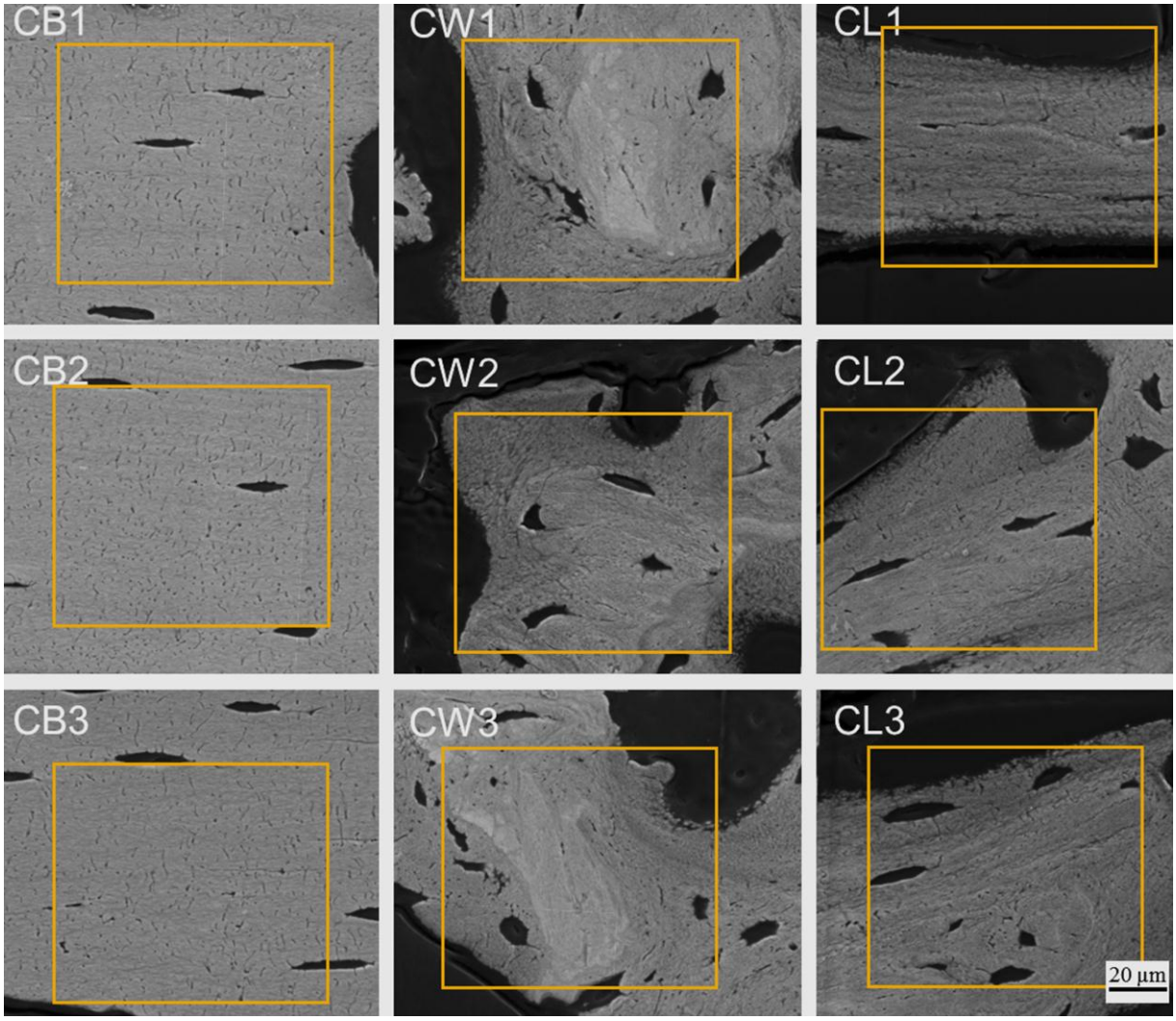

Figure 1: Backscattered electron (BSE) images of different types of bone. Cortical bone (CB), callus woven bone (CW) and newly formed callus lamellar bone (CL) can be distinguished by their degree of organization at the fibril (micrometer) level, their mineralization state (grey level) and their number and shape of osteocyte lacunae. Yellow boxes mark the areas of the later performed indents. White arrowheads depict lamellar bone layers and black arrows indicate highly mineralized woven bone islands within the callus tissue. Note that the image contrast (grey level) is adapted for better visibility of distinct bone types featuring different degrees of mineralization. Scale bar (20 µm) is valid for all images.

within the callus (Supplementary Figure 4) reveals a negative dependence between regions with high **ρ** parameter showing low mineral particle thickness **T**.

The two-dimensional distribution of **ρ** and **T** (Figure 3; see Supplementary Figure 5 for a different sample) reveals the anatomical location of the woven and lamellar bone type within the callus. CW regions exhibiting relatively thick mineral particles (T > 3 nm) together with only low mineral particle alignment (ρ < 0.4) are predominantly found in the center of the trabecular-like callus bone struts and are characteristic for callus woven bone material. At the edges of the callus bone struts, bone mineral particles are relatively thin (T < 3 nm) but show high degrees of particle orientation (ρ > 0.4) which typically runs parallel to the surface of the initially formed callus woven bone regions (Figure 3 C). These highly oriented and less mineralized regions correspond to newly formed callus lamellar (CL) bone material.

3.3 Mechanical Behavior of Different Bone Types

3.3.1 Hardness

Microindentation tests were performed on classified bone types to determine the Vickers hardness and to obtain microcracks. These microcracks were then used to evaluate crack patterns, crack lengths and consequently to obtain information on crack propagation and possible material toughening mechanisms.

Table 1 presents the hardness values of the different bone types for one individual animal. Cortical bone shows the highest hardness values (mean ± SD: 107.70 HV ± 11.94), which can be considered as a reference value for mature bone in this individual animal. In contrast, both callus bone types have lower hardness values with the lamellar regions featuring the lowest hardness (70.61 HV ± 6.74).

Figure 2

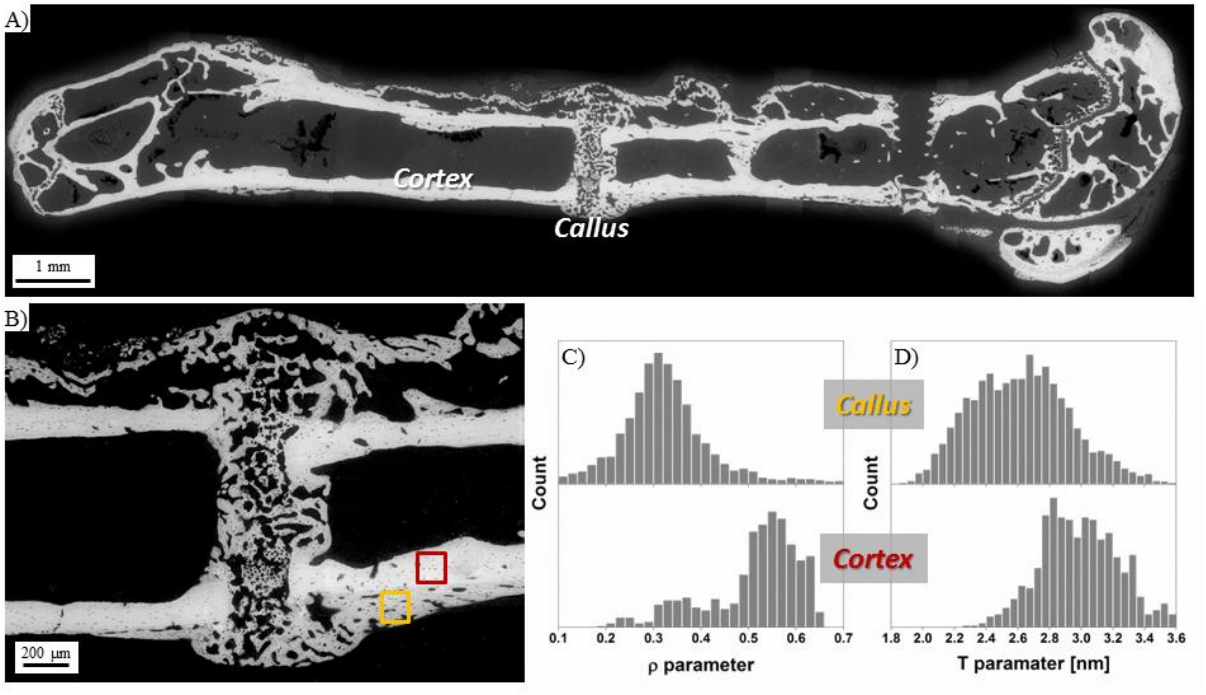

Figure 2: Backscattered electron (BSE) images of A) the osteotomized murine femur and B) the healed osteotomy. The boxes depict the representative area for SAXS measurements of the ρ and T parameter in the cortex (red) and the callus (yellow). C) Shows the distribution of ρ and D) the distribution of T in the cortex (CB) and callus region (CL and CW).

3.3.2 Crack Lengths

During microindentation crack formation and propagation was induced. The different bone types show differences in crack propagation directions and crack lengths (Table 1). Crack length values are the lowest in the CB region and the highest in the CL bone regions. The crack length shows an inverse behavior compared to the hardness of the tissue. However, the differences in terms of crack length are less pronounced than the differences in hardness values. Moreover, the values for the callus, in particular for the new lamellar bone, show extreme differences (minimum 46.65 µm, maximum 381.95 µm). However the corresponding crack pattern of the indent with the maximum value (Figure 4, CL1) shows that the measured area of lamellar bone in the callus (CL) is only about 30-40 µm in width and that the indent is close (< 5 µm) to the edge of the area. This might induce additional cracks and lower the hardness value, as there may be much softer PMMA beneath the bone strut.

3.3.3 Crack Patterns and Crack Propagation

Provoking microdamage by microindentation leads to different crack patterns within the different bone types. In CB regions very few cracks are visible (Figure 4, CB, left column). Some straight cracks typically arise at the angles of the indent that run in parallel along the lamellar orientation. Also some thin cracks around the indent angles and along the edges of the indent are visible. Compared to CB, in CL regions more and larger cracks can be observed (Figure 4, CL, middle column). Such cracks often run in parallel along the lamellar orientation. Figure 4 CL3 additionally shows two features. We had difficulties to find enough opportunities to properly position an indent within new callus lamellar bone material, as these lamellar bone packets are in the same size range as an indent. In this case, the indent is partially placed into callus woven bone (lower angle, next to roundish, irregular shaped osteocytes). In such woven bone regions no cracks are visible, whereas the callus lamellar bone material shows many cracks, both along the lamellar orientation, but also in parallel to

the indent edge. The woven bone indents (Figure 4, CW, middle column) show only few cracks that seem to surround the indent. Their crack pattern is not oriented in a specific direction.

In cortical bone, cracks preferentially propagate along the lamellar direction. Such cracks have a relatively straight appearance. In newly formed callus lamellar bone material the cracks along the lamella orientation seem to stop and reorient into another direction. The crack lines are more serrated. Especially in the upper subfigures (Figure 4, CL1 and CL2) some cracks are randomly arranged, even perpendicular to the lamellar orientation, with a very straight crack line. This gives the material a very brittle appearance. In woven bone, there is no specific crack propagation pattern recognizable. The cracks seem to be straight and even cross the interfaces of different bone packets with different mineralization states.

4 Discussion

Woven and lamellar bone can be distinguished on the microscale using BSE imaging depending on their structural appearance, their mineralization state and the architecture of their osteocyte network. Moreover nanoscopic mineral particle thickness and degree of organization, as revealed by SAXS are indicative for the different bone types (Liu, Manjubala et al. 2010). In our studies, the pre-existing cortical bone -in contrast to newly formed callus tissue- serves as a reference for mature bone. Using BSE, we find in the cortex a high degree of organization of the fibrillar bone structure together with an osteocyte network architecture characteristic for lamellar bone (Kerschnitzki, Wagermaier et al. 2011). However, in murine long bones even cortical bone shows architecture with a comparable low degree of fibril organization. Our SAXS data show the presence of a large fraction of highly oriented mineral particles, but also a smaller fraction that shows relatively poor mineral particle alignment.

This is in accordance with the known structural appearance of the murine cortex that typically consists of islands of rather poorly ordered bone material, which are surrounded by higher organized lamellar bone material (Kerschnitzki, Wagermaier et al. 2011, Shipov, Zaslansky et al. 2013). To date, it is still under debate whether rats and mice only show modeling of their long-bones during growth and development or if their intra-cortical bone material is also remodeled during later stages and to which extent such unorganized bone material is subsequently substituted with lamellar bone (Erben 1996, Shipov, Zaslansky et al. 2013).

The morphological and ultrastructural description of the callus material in mice also reveals the woven and lamellar bone type, which is in good accordance with other studies where a less organized woven bone type serves as a scaffold for more organized lamellar bone (Liu, Manjubala et al. 2010, Kerschnitzki, Wagermaier et al. 2011). The degree of mineralization as revealed by BSE shows differences within the callus tissue: higher mineralized (lighter grey) woven bone islands surrounded by less mineralized (darker grey) lamellar bone areas. SAXS measurements show that callus woven bone material features relatively thick mineral particles, probably due to their high degree of mineralization, together with a low degree of particle orientation. Such woven bone islands are surrounded by highly organized callus lamellar bone material in a lower mineralization state. Therefore, in younger callus lamellar bone, mineral particles are found to be rather thin (low T) but show a high degree of organization, predominantly with an orientation that runs parallel along the surface of the primarily formed woven bone islands. Such ultrastructural correspondence between callus woven and callus lamellar bone is in agreement with the current understanding of primary woven bone formation which serves as an endogenous substrate for subsequent deposition of highly organized bone material along the woven bone surface (Kerschnitzki, Wagermaier et al. 2011, Kerschnitzki, Wagermaier et al. 2011). It has been shown that during bone healing in rat a bony bridging occurs at first in the endosteal callus (Hoerth, Seidt, et al. 2014), enabling load transfer along the bone axis. The spatial distribution of the different structural types found in

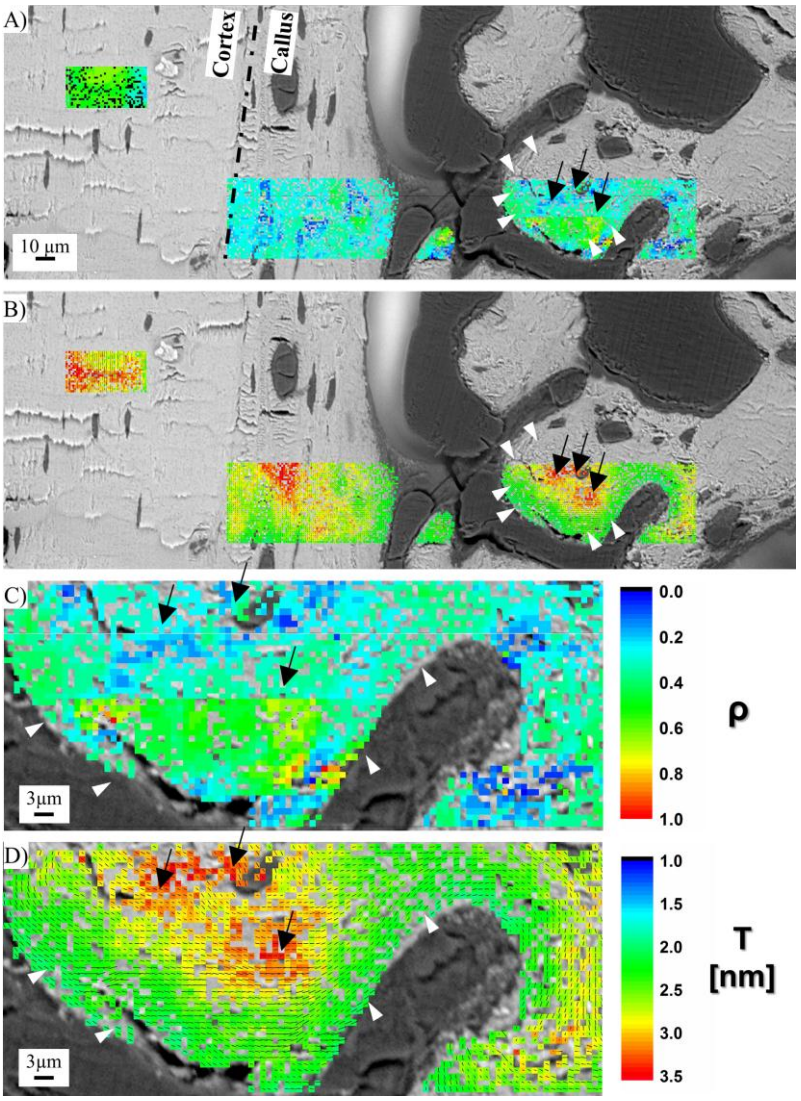

Figure 3: Scanning small angle X-ray scattering results of cortex and callus. A) Backscattered electron image depicts the ultrastructure and the mineralization level of cortex and callus. Light grey: mineralized regions. Dark grey: PMMA/soft tissue. Degree of orientation (ρ parameter) is represented color-coded. B) Mean particle thickness (T parameter) is represented color-coded. C) & D) are magnified subsections of the degree of orientation (ρ parameter) and the mean particle thickness (T parameter) shown in A) and B) respectively. The range of ρ and T parameter values are color-coded and overlaid on the BSE image. Black arrows show typical woven bone (CW) with poorly oriented architecture. White filled arrow heads depict new lamellar bone (CL) material that surrounds these CW islands e (black arrows).

the callus of the presented mice could be the result of biomechanical environment, but to understand the relation a more detailed study with individuals from different time points would be needed.

The different bone types show distinct hardness and crack propagation mechanisms, due to differences in mineral particle size and orientation at the nanoscale and fibril orientation at the micrometer scale. The lamellar cortex with highly oriented and relatively thick mineral particles shows the highest Vickers hardness values whereas the callus bone material typically has lower values. In particular, the highly mineralized but poorly oriented woven bone islands within the callus feature a hardness which is still greater than those of less mineralized (small T) but highly oriented lamellar bone layers surrounding such islands. A different study on ovine fracture healing showed a generally very heterogeneous mechanical behavior of callus tissue with increasing tissue stiffness over healing time (Manjubala, Liu et al. 2009). Our data implies that this heterogeneity derives from the different callus bone types that possess distinct hardness values. Manjubala et al. also found that during the late healing stages the callus stiffness still remained relatively low, roughly at 60% of that of the cortex (Manjubala, Liu et al. 2009). We find a similar trend with the callus tissue hardness being approximately only 70% of that of the cortex. Different theoretical models predict a strong dependence of mechanical behavior of tissues depending on the size of the mineral particles embedded in the collagenous matrix (Bar-On and Wagner 2012, Gupta, Krauss et al. 2013). Our data on the particle thickness (T) together with findings from another study investigating the particle length (L) in healing rat bone (Hoerth, Seidt et al. 2014) show that during healing (increasing callus tissue age) mineral particle sizes typically change from on average short and thick to long and thin particles. According to the above mentioned models, such alteration of mineral particle size may contribute to differences in mechanical properties of the different bone types.

It is still under discussion, whether material toughness can be directly measured and accurately quantified with Vickers indentation fracture (VIF) test (Kruzic, Kim et al. 2009). However, crack lengths measurements can be a first step in understanding mechanisms providing toughness in materials with varying degree of organization at the micro- and nanostructural level. We found that cortical bone has short crack lengths (Table 1), whereas the callus regions exhibit comparable longer crack lengths with the callus lamellar bone having typically the longest cracks. Based on this, we could speculate that toughness would be highest in cortical bone and the lowest in callus lamellar bone. But such a hypothesis has to be proven by more detailed mechanical measurements as e.g. described in Kruzic, Kim et al. 2009.

Different crack patterns also indicate different behavior in response to crack propagation due to indentation. Both, cortical lamellar bone and callus lamellar bone show oriented crack propagation along the lamellar direction. However, callus lamellar bone has higher crack lengths, indicating a poorer resistance to cracking. Additionally to such oriented cracks, both cortical and callus lamellar bone show cracks at the borders of the remaining indent. In contrast, callus woven bone shows randomly oriented cracks in accordance with the low degree of tissue organization. The different crack propagation patterns within the different bone types indicate different toughening mechanisms of the bone material. There are structural features of the bone which lead to an increase in toughness (Wagermaier, Klaushofer, Fratzl 2015) and Ritchie et al. distinguished between intrinsic and extrinsic factors (Launey, Buehler et al. 2010, Ritchie 2011). The extrinsic factors at the hierarchical levels at the micro and macro scale lead to toughening mechanisms such as crack deviation, crack bridging and microcracking and all those mechanisms slow down crack propagation (Koester, Ager et al. 2008, Launey, Buehler et al. 2010, Ritchie 2011). Both cortical and callus lamellar bone material exhibit cracks that run along the lamellar orientation where

crack bridging can contribute to energy dissipation. Thus, young and poorly mineralized callus lamellar bone already shows crack propagation mechanisms which are similar to those of mature cortical bone. However, the callus lamellar bone also shows some cracks that run randomly or and sometimes perpendicular to the lamellar orientation and particularly those cracks have relatively straight crack paths without any recognizable crack bridging. Those cracks are very similar to cracks found within callus woven bone material.

Toughness values determined from cracks introduced via indentation techniques are known to show high variability and should differ at least by a factor of three to conclude a significant difference in actual toughness (Kruzic, Kim et al. 2009). In our measurements, we do not see such significant differences in crack length. There is no simple correlation between crack length and toughness, because of two contradicting effects: (i) crack propagation consumes energy before failure, increasing toughness and (ii) crack propagation also is the initial step of total failure. From a fibril-orientation-point of view together with the known crack bridging mechanisms at interfaces between lamellae one would expect highest toughness values for the lamellar regions. Our data show an increasing crack length in the following order: cortex, callus woven and callus lamellar regions. We can see a positive correlation between the degree of mineralization and hardness: the lamellar cortex is highly mineralized and shows high hardness values whereas the lamellar callus shows low mineralization together with low hardness. We assume highest toughness in the lamellar cortex regions, in which we find lowest crack lengths together with crack bridging by fibers or ligaments crossing the interfaces between lamellae.

There are limitations in performing and evaluating the micro-indentation tests in order to obtain hardness and toughness values. In general, it was difficult to find lamellar callus regions which were large enough for proper indentation. Such trabecular-like struts are often thin, such that the measurements may be influenced by the PMMA-embedding in their

Figure 4

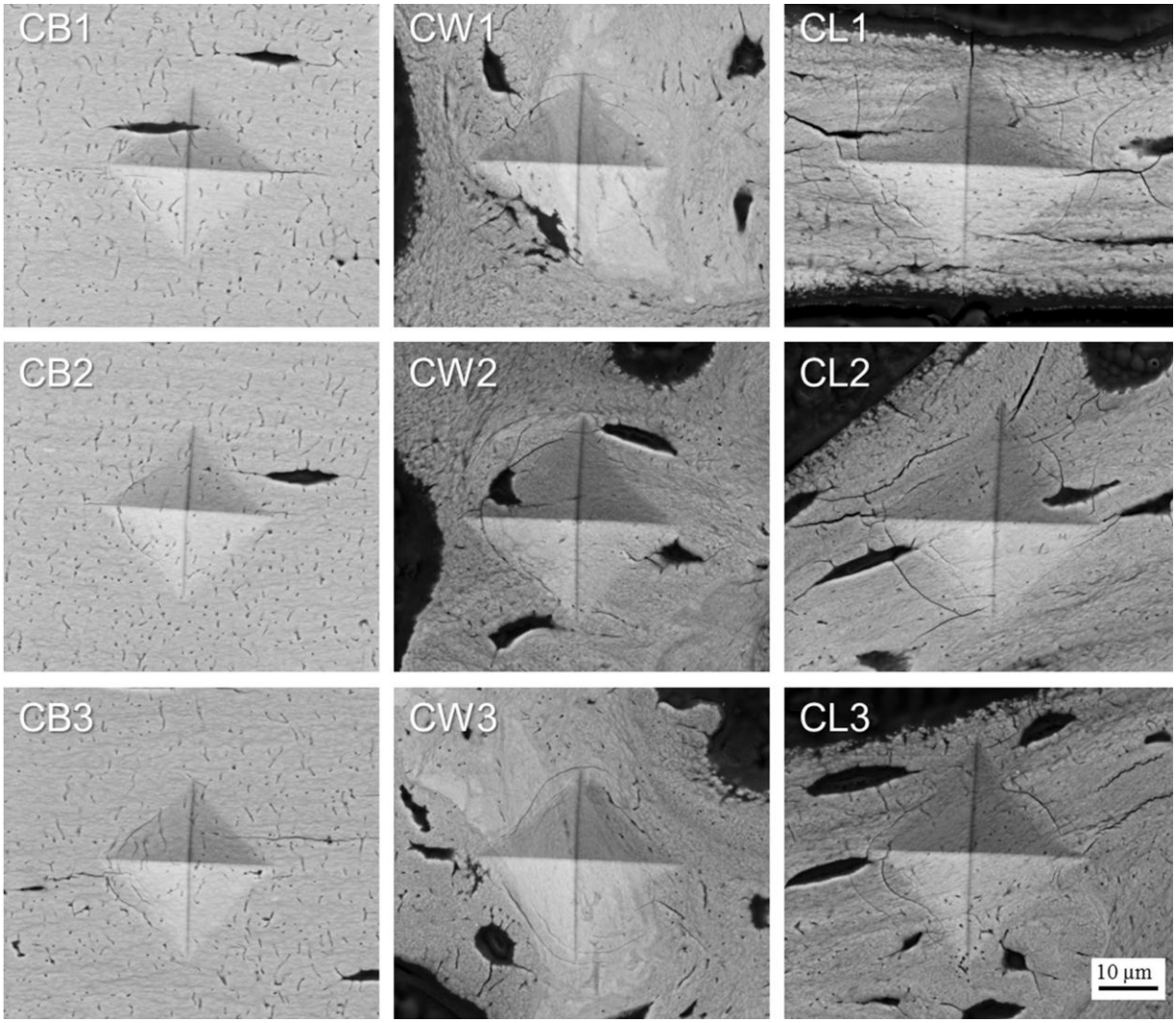

Figure 4: Backscattered electron images showing examples of microindents in different bone types (CB: cortical bone, CW: callus woven bone, CL: callus lamellar bone). White arrowheads depict lamellar bone layers and black arrows indicate highly mineralized woven bone islands within the callus tissue. Note that the image contrast (grey level) is adapted for better visibility of indentation cracks and corresponding crack patterns.

vicinity. Moreover, within the callus, woven bone and lamellar bone are in close contact such that layers of lamellar structured bone are wrapped around islands of poorly organized woven bone within a small space. Therefore, we cannot rule out the possibility that indentation measurements of the different bone types in the callus are influenced by such intertwining. Deducing the toughness from the crack lengths holds further difficulties. The crack lengths were determined visually. We compared pre- and post-indented BSE images to avoid including pre-existing cracks. Nevertheless we cannot exclude, that there was further crack formation and propagation between the two imaging steps which was not induced by indentation. Alignment of the indent diameter with the bone lamellae would improve consistency of measurements. Furthermore, very thin and small cracks at the border of indents within cortical bone counted the same as large and deep cracks within the callus bone. Therefore these small cracks were given more weight in our analysis, as we did not take the crack thickness into account. Nevertheless there are trends visible which indicate that not only hardness, but also toughness differs between the different bone types.

5 Conclusions

Combining back-scattered electron microscopy imaging, synchrotron SAXS and microindentation, we described correlations between nanoscopic bone material structure and microscopic mechanical properties in regions with different fibrillar organization and varying mineral content within healing murine bone. We showed that in the bony callus, highly mineralized but poorly organized woven bone is present together with lamellar bone layers, which are typically deposited along the surface of such woven bone islands. We find a negative correlation between the degree of mineral particle orientation and mineral particle thickness within the callus tissue. Thus, woven bone features thicker, but less organized mineral particles whereas callus lamellar bone layers show thinner mineral particles with a higher degree of orientation. These different bone types also possess distinct hardness and

characteristic cracking patterns which derive from their specific micro- and nanostructure. Lamellar bone in the cortex regions shows high hardness and presumably high toughness compared to the developing bone in the callus region. This shows that structural features at different hierarchical levels and the degree of mineralization in bone may have an impact on the hardness and toughness of the tissue.

6 Acknowledgements

We thank Dr. Bettina Kruck for performing the osteotomy surgeries and Marzena Princ for helping with tissue processing. We acknowledge the European Synchrotron Radiation Facility (ESRF) in Grenoble, France for granting us beamtime. This study was partially supported by the German Research Foundation (Deutsche Forschungsgemeinschaft FG 2165, WI 3761/4-1, DU 298/21-1).

7 References

Bar-On, B. and H. D. Wagner (2012). "Elastic modulus of hard tissues." Journal of biomechanics **45**(4): 672-678.

Benecke, G., W. Wagermaier, C. H. Li, M. Schwartzkopf, G. Flucke, R. Hoerth, I. Zizak, M. Burghammer, E. Metwalli, P. Muller-Buschbaum, M. Trebbin, S. Forster, O. Paris, S. V. Roth and P. Fratzl (2014). "A customizable software for fast reduction and analysis of large X-ray scattering data sets: applications of the new DPDAK package to small-angle X-ray scattering and grazing-incidence small-angle X-ray scattering." Journal of Applied Crystallography **47**: 1797-1803.

Cipitria, A., C. Lange, H. Schell, W. Wagermaier, J. C. Reichert, D. W. Hutmacher, P. Fratzl and G. N. Duda (2012). "Porous scaffold architecture guides tissue formation." Journal of Bone and Mineral Research **27**(6): 1275-1288.

Cowin, S. C. (2001). Bone mechanics handbook, CRC press.

Currey, J. (2003). "The many adaptations of bone." Journal of biomechanics **36**(10): 1487-1495.

Currey, J. D. (2002). Bones: structure and mechanics, Princeton university press.

Erben, R. G. (1996). "Trabecular and endocortical bone surfaces in the rat: Modeling or remodeling?" Anatomical Record **246**(1): 39-46.

Ferretti, M., C. Palumbo, M. Contri and G. Marotti (2002). "Static and dynamic osteogenesis: two different types of bone formation." Anatomy and embryology **206**(1-2): 21-29.

Fratzl, P. (1994). "Statistical model of the habit and arrangement of mineral crystals in the collagen of bone." Journal of Statistical Physics **77**(1-2): 125-143.

Fratzl, P., N. Fratzl-Zelman, K. Klaushofer, G. Vogl and K. Koller (1991). "Nucleation and Growth of Mineral Crystals in Bone Studied by Small-Angle X-Ray-Scattering." Calcified Tissue International **48**(6): 407-413.
Fratzl, P., H. Gupta, E. Paschalis and P. Roschger (2004). "Structure and mechanical quality of the collagen–mineral nano-composite in bone." Journal of materials chemistry **14**(14): 2115-2123.
Fratzl, P., S. Schreiber and K. Klaushofer (1996). "Bone mineralization as studied by small-angle X-ray scattering." Connective Tissue Research **34**(4): 247-254.
Fratzl, P. and R. Weinkamer (2007). "Nature's hierarchical materials." Progress in Materials Science **52**(8): 1263-1334.
Gupta, H., S. Krauss, M. Kerschnitzki, A. Karunaratne, J. Dunlop, A. Barber, P. Boesecke, S. Funari and P. Fratzl (2013). "Intrafibrillar plasticity through mineral/collagen sliding is the dominant mechanism for the extreme toughness of antler bone." Journal of the mechanical behavior of biomedical materials **28**: 366-382.
Gupta, H. S., P. Fratzl, M. Kerschnitzki, G. Benecke, W. Wagermaier and H. O. Kirchner (2007). "Evidence for an elementary process in bone plasticity with an activation enthalpy of 1 eV." Journal of the Royal Society Interface **4**(13): 277-282.
Gupta, H. S., J. Seto, W. Wagermaier, P. Zaslansky, P. Boesecke and P. Fratzl (2006). "Cooperative deformation of mineral and collagen in bone at the nanoscale." Proceedings of the National Academy of Sciences **103**(47): 17741-17746.
Hernandez, C., R. Majeska and M. Schaffler (2004). "Osteocyte density in woven bone." Bone **35**(5): 1095-1099.
Hirose, S., M. Li, T. Kojima, P. H. L. de Freitas, S. Ubaidus, K. Oda, C. Saito and N. Amizuka (2007). "A histological assessment on the distribution of the osteocytic lacunar canalicular system using silver staining." Journal of bone and mineral metabolism **25**(6): 374-382.
Hoerth, R. M., B. M. Seidt, M. Shah, C. Schwarz, B. M. Willie, G. N. Duda, P. Fratzl and W. Wagermaier (2014). "Mechanical and structural properties of bone in non-critical and critical healing in rat." Acta biomaterialia **10**(9): 4009-4019.
Imbeni, V., J. J. Kruzic, G. W. Marshall, S. J. Marshall and R. O. Ritchie (2005). "The dentin-enamel junction and the fracture of human teeth." Nat Mater **4**(3): 229-232.
Kerschnitzki, M. (2012). Bone material characteristics influenced by osteocytes, Humboldt-Universität zu Berlin, Mathematisch-Naturwissenschaftliche Fakultät I.
Kerschnitzki, M., W. Wagermaier, Y. Liu, P. Roschger, G. N. Duda and P. Fratzl (2011). "Poorly ordered bone as an endogenous scaffold for the deposition of highly oriented lamellar tissue in rapidly growing ovine bone." Cells Tissues Organs **194**(2-4): 119-123.
Kerschnitzki, M., W. Wagermaier, P. Roschger, J. Seto, R. Shahar, G. N. Duda, S. Mundlos and P. Fratzl (2011). "The organization of the osteocyte network mirrors the extracellular matrix orientation in bone." Journal of structural biology **173**(2): 303-311.
Koester, K. J., J. Ager and R. Ritchie (2008). "The true toughness of human cortical bone measured with realistically short cracks." Nature materials **7**(8): 672-677.
Kruck, B., G. Duda, S. Damerow, F. Wichlas, S. Tsitsilonis and B. Willie (2013). Fixation Stiffness Modulates the Efficacy of Sclerostin-Neutralizing Antibody Treatment during Bone Healing. Journal of Bone and Mineral Research, Wiley-Blackwell 111 River St, Hoboken 07030-5774, NJ USA.
Kruzic, J., D. Kim, K. Koester and R. Ritchie (2009). "Indentation techniques for evaluating the fracture toughness of biomaterials and hard tissues." Journal of the Mechanical Behavior of Biomedical Materials **2**(4): 384-395.
Landis, W. J., K. J. Hodgens, J. Arena, M. J. Song and B. F. McEwen (1996). "Structural relations between collagen and mineral in bone as determined by high voltage electron microscopic tomography." Microscopy Research and Technique **33**(2): 192-202.

Landis, W. J., M. J. Song, A. Leith, L. McEwen and B. F. McEwen (1993). "Mineral and organic matrix interaction in normally calcifying tendon visualized in 3 dimensions by high-voltage electron-microscopic tomography and graphic image-reconstruction." Journal of Structural Biology **110**(1): 39-54.
Launey, M. E., M. J. Buehler and R. O. Ritchie (2010). "On the Mechanistic Origins of Toughness in Bone." Annual Review of Materials Research, Vol 40 **40**: 25-53.
Liu, Y. F., I. Manjubala, H. Schell, D. R. Epari, P. Roschger, G. N. Duda and P. Fratzl (2010). "Size and Habit of Mineral Particles in Bone and Mineralized Callus During Bone Healing in Sheep." Journal of Bone and Mineral Research **25**(9): 2029-2038.
Manjubala, I., Y. Liu, D. R. Epari, P. Roschger, H. Schell, P. Fratzl and G. Duda (2009). "Spatial and temporal variations of mechanical properties and mineral content of the external callus during bone healing." Bone **45**(2): 185-192.
Martin, R. and D. Boardman (1993). "The effects of collagen fiber orientation, porosity, density, and mineralization on bovine cortical bone bending properties." Journal of biomechanics **26**(9): 1047-1054.
McKibbin, B. (1978). The biology of fracture healing in long bones. J Bone Joint Surg [Br.
Mullins, L. P., M. S. Bruzzi and P. E. McHugh (2007). "Measurement of the microstructural fracture toughness of cortical bone using indentation fracture." J Biomech **40**(14): 3285-3288.
Pabisch, S., W. Wagermaier, T. Zander, C. Li and P. Fratzl (2013). "Imaging the nanostructure of bone and dentin through small- and wide-angle X-ray scattering." Methods in enzymology **532**: 391-413.
Peterlik, H., P. Roschger, K. Klaushofer and P. Fratzl (2006). "From brittle to ductile fracture of bone." Nature materials **5**(1): 52-55.
Reznikov, N., R. Shahar and S. Weiner (2014). "Bone hierarchical structure in three dimensions." Acta biomaterialia **10**(9): 3815-3826.
Rho, J.-Y., T. Y. Tsui and G. M. Pharr (1997). "Elastic properties of human cortical and trabecular lamellar bone measured by nanoindentation." Biomaterials **18**(20): 1325-1330.
Rinnerthaler, S., P. Roschger, H. F. Jakob, A. Nader, K. Klaushofer and P. Fratzl (1999). "Scanning small angle X-ray scattering analysis of human bone sections." Calcified Tissue International **64**(5): 422-429.
Ritchie, R. O. (2011). "The conflicts between strength and toughness." Nature Materials **10**(11): 817-822.
Röntgen, V., R. Blakytny, R. Matthys, M. Landauer, T. Wehner, M. Göckelmann, P. Jermendy, M. Amling, T. Schinke and L. Claes (2010). "Fracture healing in mice under controlled rigid and flexible conditions using an adjustable external fixator." Journal of Orthopaedic Research **28**(11): 1456-1462.
Roschger, P., H. S. Gupta, A. Berzlanovich, G. Ittner, D. W. Dempster, P. Fratzl, F. Cosman, M. Parisien, R. Lindsay, J. W. Nieves and K. Klaushofer (2003). "Constant mineralization density distribution in cancellous human bone." Bone **32**(3): 316-323.
Shapiro, F. (2008). "Bone development and its relation to fracture repair. The role of mesenchymal osteoblasts and surface osteoblasts." Eur Cell Mater **15**(53): e76.
Shipov, A., P. Zaslansky, H. Riesemeier, G. Segev, A. Atkins and R. Shahar (2013). "Unremodeled endochondral bone is a major architectural component of the cortical bone of the rat (Rattus norvegicus)." Journal of Structural Biology **183**(2): 132-140.
Wagermaier, W., K. Klaushofer and P. Fratzl (2015). "Fragility of bone material controlled by internal interfaces." Calcified tissue international **97**(3): 201-212.
Weiner, S. and H. D. Wagner (1998). "The material bone: structure-mechanical function relations." Annual Review of Materials Science **28**(1): 271-298.
Zysset, P. K., X. E. Guo, C. E. Hoffler, K. E. Moore and S. A. Goldstein (1999). "Elastic modulus and hardness of cortical and trabecular bone lamellae measured by nanoindentation in the human femur." Journal of biomechanics **32**(10): 1005-1012.